Express Polymer Letters Vol.19, No.10 (2025) 1012–1026
Available online at www.expresspolymlett.com
https://doi.org/10.3144/expresspolymlett.2025.76

Research article

Electrospinning of epoxy fibers: Mechanical properties and failure mechanisms

Mark Shneider[1], *Xiaomeng Sui*[2], *Iddo Pinkas*[2], *Ulyana Shimanovich*[1], *Israel Greenfeld*[1], *Daniel Wagner*[1*]

[1]Department of Molecular Chemistry and Materials Science, Weizmann Institute of Science, 7610001 Rehovot, Israel
[2]Chemical Research Support, Weizmann Institute of Science, 761001 Rehovot, Israel

Received 14 April 2025; accepted in revised form 23 June 2025

Abstract. Electrospinning is a widely used technique for manufacturing nanofibers from polymers. The formation of continuous fibers during the drawing of a viscous solution typically depends on entanglements between polymer chains, making thermoplastics the preferred choice. In this study, we have shown that thermosetting polymers such as epoxy, which have crosslinked covalent bonds, can also be electrospun. The resulting fibers have diameters ranging from 150 nm to 6 µm. Tensile mechanical properties of fibers with diameters varying between 410 nm and 4 µm are compared with those of molded epoxy bulk. The electrospun fibers exhibit approximately 555% higher strength, 300% greater stiffness, and a strain of about 109% compared to the equivalent properties of bulk epoxy. When compared with brittle molded bulk, these fibers showed ductile properties. We also observed a correlation between the fiber diameter and the mechanical properties. The molecular morphology of the fibers was monitored and analyzed using polarized micro-Raman spectroscopy to detect molecular orientation. A comparison with epoxy fibers of different diameters from previous studies was conducted to better understand the size effect. This study shows, explains and models the evolution of epoxy molecular morphology from the solution (soft matter) to fiber (solid-state), explaining the transition from brittle to ductile in epoxy fibers, and clarifying the molecular mechanisms that lead to improved mechanical properties.

Keywords: *epoxy, nanofibers, fracture toughness, electrospinning, mechanical properties*

1. Introduction

Electrospinning is a versatile fiber preparation technique widely used in scientific research for its ability to create fibers with nanometric dimensions [1, 2]. In industry, there is growing interest in utilizing these nanofibers in applications such as filtration due to their capability to precisely control mesh porosity, which can reach down to nanometric scales, potentially increasing particle penetration selectivity [3, 4]. Recently, electrospinning has also gained popularity in biomedical applications, including wound dressings, coatings for endovascular treatments, and more, primarily due to the excellent biocompatibility of fibers when formed into a mesh morphology [5, 6].

To initiate the electrospinning process, a solution of polymer dissolved in a dielectric solvent is required, although the process can also use molten polymer [2, 7]. This solution must be fluid enough to flow through a thin nozzle, form a Taylor cone under an electric field, and maintain its integrity during elongation to produce continuous fibers [2]. A wide range of thermoplastic polymer materials can be electrospun, and even, more recently, natural proteins [8, 9]. The primary mechanism for fiber formation involves preparing a viscous solution or melt of

*Corresponding author, e-mail: daniel.wagner@weizmann.ac.il

long, entangled polymer chains. These entanglements act as anchoring points between chains, preventing the solution from being torn apart during the electrostatic stretching process [10].

Epoxy, the focus of this work, is a two-component thermoset polymer. When mixed with a curing agent, typically an amine-based molecule, it undergoes crosslinking and solidifies [11]. Initially, the epoxy molecules are short, but as crosslinking initiates, their molecular weight increases, typically forming clusters in a three-dimensional tree-like morphology [12, 13].

Epoxy is used in a wide range of applications, mainly in composites [14], adhesives [15], and coatings [16], but rarely as a fiber, because of the challenges in controlling the curing reaction under drawing conditions. Previous studies on mechanically drawn epoxy fibers, having diameters ranging from 10 to 200 μm, have shown significant changes in mechanical properties compared to molded bulk epoxy [17]. These epoxy fibers exhibited ductile properties, with strains up to 116%, a high strength at break of 234 MPa, and an elastic modulus of 2.5 GPa [17]. Electrospun fibers in the 1.5 to 20 μm diameter range have exhibited even better mechanical characteristics [18]. In contrast, bulk epoxy typically displays brittle properties, with a strength at break around 68 MPa and a fracture strain of only up to 12% [17]. The unusual mechanical properties of mechanically drawn and electrospun fibers have been attributed to the approximately unidirectional rearrangement of the molecular structure induced by mechanical drawing [19]. Electrospinning, with its strong electrostatic stretching, has the potential to produce even thinner fibers and reach the nanometric scale, with potentially superior mechanical properties [20, 21].

In this research, epoxy fibers with diameters ranging from 150 nm to 6 μm were prepared by electrospinning and subsequently mechanically tested. The strain, strength, and stiffness of the fibers were measured by tensile testing, and the results were compared with data from previous studies to assess the impact of fiber diameter on mechanical properties. The molecular morphology was analyzed by polarized micro-Raman spectroscopy to assess molecular orientation. Additionally, the molecular morphology of the solution in its liquid state prior to spinning and of the spun fibers (in their solid state) was modeled. We propose a mechanism that explains how ductility arises in the fiber.

2. Materials and methods

2.1. Solution preparation

The epoxy used in this study was diglycidyl ether of bisphenol-A (DGEBA), specifically resin EP828 (molecular weight 340 g/mol), with hardener EP304 (PolymerG, Israel). The hardener, a polyether triamine, was mixed with the epoxy in a weight ratio of 100:42 epoxy: hardener.

N-*N*-dimethylformamide (DMF) and tetrahydrofuran (THF), both purchased from Sigma Aldrich, Israel, were used as solvents for the epoxy. The solvents were mixed in a weight ratio of 2:8 and then immediately combined with the epoxy mixture, making up 80% of the total solution weight. DMF, with its high dielectric constant of 36.7 and boiling point of 153 °C, was selected to enhance the electrical responsiveness of the solution. THF, with a dielectric constant of 7.6 and a boiling point of 66 °C, acted as a volatile component, promoting rapid fiber solidification during spinning.

The epoxy-solvent mixture was vigorously stirred for 20 min using a conditioning mixer, then aliquoted into bottles and placed in an oven at 55 °C for 294 h. Following the solution preparation, the bottles were removed and stored at –18 °C to quench the curing reaction. Before being used in electrospinning, the solutions were thawed to room temperature and stirred magnetically at 300 rpm for 15 min.

2.2. Electrospinning

Our homemade electrospinning system (Figure 1a) included a syringe pump (Fusion 4000, Chemyx Inc., USA) and a DC power supply (PS/FC50R02, Glassman High Voltage, USA). The nozzle consisted of a blunt cannula needle with internal and longitudinal dimensions of 0.81×25 mm (21G, MonoJect, Covidian, Ireland) connected to a disposable 10 mL syringe (Norm-Ject, Merck, Israel). The fiber collector was an aluminum net with a 15×15 mm cell size. The power supply unit was connected to a 100 mm long and 2 mm diameter copper rod electrode, positioned 10 mm behind the net, with the net itself placed 190 mm away from the nozzle. The electrospinning process was conducted at room temperature.

The goal was to direct the fiber towards the electrode while ensuring it was collected on the aluminum net just before reaching the electrode. To optimize the process, parameters including the solution flow rate, electric field strength, nozzle diameter, and the

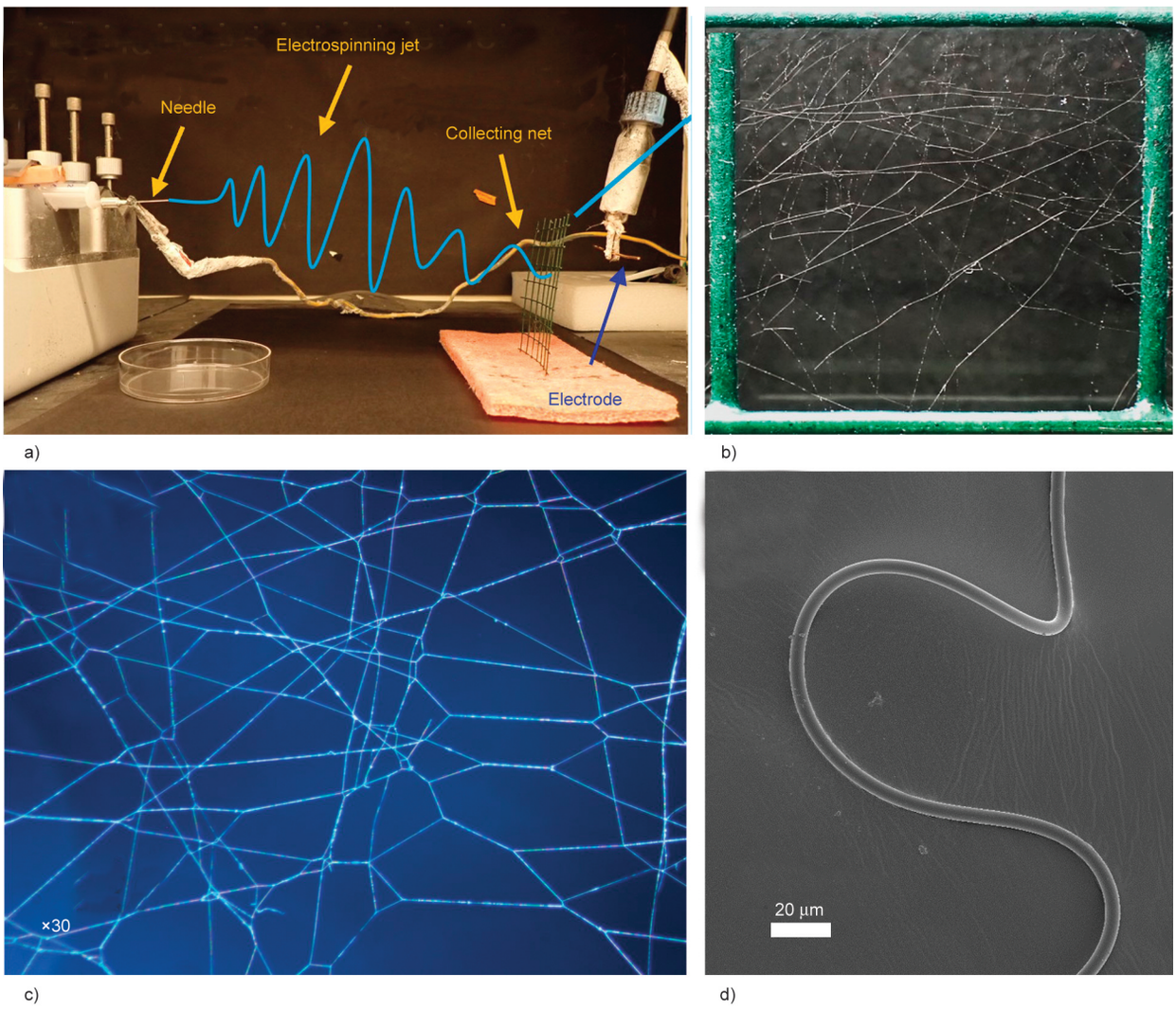

Figure 1. a) The nozzle to screen distance is 190 mm, and the electrode is 10 mm behind the screen, b) electrospun epoxy fibers deposited on an aluminum net, c) electrospun fibers by optic microscopy, d) scanning electron micrograph (SEM) of a single electrospun micro-fiber prepared from epoxy/(THF/DMF) solution, with epoxy concentration of 20 wt%.

distance between the electrode and the net were adjusted. Fibers were also collected on transparent glass slides, which were inserted into the chamber during the electrospinning process and observed under an optical microscope. The primary focus of optimization was to minimize bead formation and achieve uniform fibers, as shown in Figures 1b–1d. Typically, increasing the solution viscosity led to a reduction in bead formation. The rheological properties, including the dependence of the molar mass and viscosity on curing time and conditions, were discussed in detail in our previous work [21], and describe how to achieve a stable electrospinning process.

Electrospinning of the epoxy/(THF/DMF) solution was carried out at a feeding rate of 0.5 mL/h, with an applied voltage of 19–21 kV, at ambient temperature of 24 °C and humidity range of 45±5% controlled by local air-conditioning, resulting in fibers such as depicted in Figure 1d. This solution enabled the production of nanofibers. All fibers were collected on the aluminum net (Figure 1b), allowed to rest for 16 h, then subjected to vacuum for 24 h to evaporate any residual solvents, and finally cured in an oven at 100 °C for 6 h. Previous studies examining solvent residuals using differential scanning calorimetry (DSC) analysis did not show any significant observations. Therefore, it was assumed that the amount of solvent trapped in the matrix was negligible [18].

2.3. Polarized micro-Raman spectroscopy

All samples were analyzed using a Horiba LabRAM HR Evolution micro-Raman spectrometer (Horiba, France), utilizing a 633 nm excitation wavelength. The spectrometer was equipped with four laser lines

(325, 532, 633, and 785 nm). The laser spot size was typically less than 1 μm when using a 50× objective (L M PlanFL N, NA = 0.5 Olympus, Japan) and less than 0.5 μm using a 100× objective (MPlanFL N, NA = 0.9 Olympus, Japan). The system featured an 800 mm focal length spectrograph allowing for high resolution and low stray light with interchangeable gratings and an open electrode, front-illuminated, cooled CCD detector. Samples were placed under a modular microscope (Olympus BX-FM) and observed using the above-mentioned objectives.

To measure the molecular orientation in drawn epoxy fibers, a half-wave plate was used on the excitation laser, and an analyzer was positioned in the collection path to measure the parallel (*ZZ*) and perpendicular (*XX*) polarized Raman signal of the fiber samples (Figure 2a). A depolarizer was inserted in the collected light path beyond the analyzer to mitigate the polarization sensitivity of the spectrograph grating and CCD detector. For depth profiling within samples, a motorized stage was employed, and the confocal configuration of the microscope ensured that signals from a limited depth of focus were analyzed by the spectrograph. The depth resolution varied as the objective focused deeper into the material. Due to the curvature of the fiber surface, the Raman signal intensity increased with deeper focusing, peaking at a certain depth. Therefore, all measurements, except for the depth scan (*Y* direction), were performed at a depth of 1 μm.

A molded epoxy bulk sample was used as a reference for non-polarized material. This reference was prepared by molding the solution and allowing it to rest during the entire curing process, ensuring that no external forces were applied, thereby minimizing stress within the matrix. Consequently, minimal intensity variations were measured across different polarizations. By analyzing the polarizations in the *Z* and *X* directions, intensity differences were identified and used to calibrate any bias introduced during the polarizing system setup assembly [19].

The analysis involved taking readings along the fiber at intervals of 2.5 μm, covering a total length of 100 μm, as illustrated in Figure 2b. This approach enabled the creation of a Raman intensity profile along the fiber. The same procedure was applied to the molded bulk epoxy for comparison (Figure 2c). The Raman spectra obtained were used to determine the intensity of the Raman peaks.

2.4. Fiber mechanical testing

2.4.1. Tensile testing device

To prepare samples for tensile testing, each fiber (in a diameter range of 1.5–7 μm) was cut to yield a

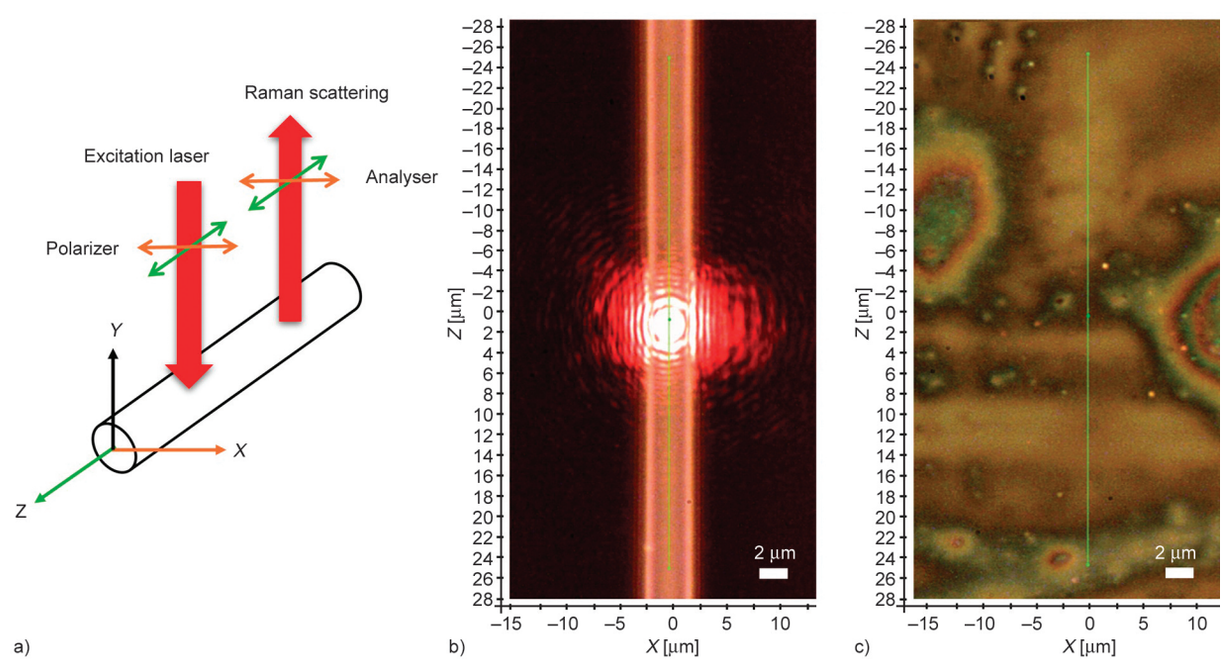

Figure 2. a) Schematic description of the micro-polarized Raman scattering setup for measuring the shift in energy of light scattered by the epoxy fiber. The specimen was tested in polarization vectors of *X* and *Z*. The micro-polarized visible excitation laser spot size, generated using a 100× objective, was shined onto the surface of epoxy fiber (b) and molded bulk (c). The longitudinal analysis readings, marked with a green line, were performed at a distance of 2.5 μm for every step over a length of 100 μm along the sample.

gauge length of 10 mm and secured to a frame. This method ensured that the fiber remained aligned with the test direction and was protected from damage during handling. Initially, the fiber ends were affixed to the frame with tape. A small drop of fast-drying epoxy was then applied to each end, which was subsequently covered with a small piece of cardboard to hold it securely in place.

Tensile tests were performed using an Instron 5965 universal testing system (UK) equipped with a 10 N load cell. Prior to testing, the diameter of each fiber was measured at three points along its length using an optical microscope, and the average diameter was calculated. The fiber specimen was then clamped into the grips of the tensile testing machine, and the cardboard frame borders were carefully cut away before testing began. A strain rate of 1 mm/min was applied, and the force was recorded until the fiber broke. This testing procedure provided the mechanical properties of the fiber, including maximum stress, strain at failure, Young's modulus, and toughness.

2.4.2. Tensile push-to-pull device

Measuring the tensile properties of sub-micron fibers requires the use of a highly sensitive load cell. To enable detailed observation of the fibers during tensile testing, such a sensitive custom tool was designed, built and adapted to function within the scanning electron microscope (SEM) chamber (Figure 3). SEM monitoring allows precise observation and analysis of failure mechanisms.

This custom push-to-pull tensile tester was made of a double cantilever beam (Kleindiek, Germany) (Figure 3a). The sample preparation procedure (Figure 3d) involved attaching a piece of aluminum foil to a base, followed by applying carbon tape on top of the foil to create a surface for adhering the fiber. A section of the collector net, used during the electrospinning process, containing the fibers, was placed on the carbon tape so that the ends of a fiber adhered to the tape. A drop of epoxy was then applied between the gap and the carbon tape, securing the fiber to the testing device. Once the epoxy was cured, the frame was removed, leaving one fiber affixed to the device.

The testing device was then positioned inside the SEM chamber (Zeiss LEO Supra 55VP, Germany). A nano-manipulator (Kleindiek, with Nanotechnik controller, model NanoControl NC-2-3, Germany) was aligned parallel to the cantilever beam and used to apply strain to the fiber by moving along its longitudinal direction, as shown in Figure 3a. The strain rate during testing was 46 µm/min. This setup allowed us to monitor both strain and tensile stress up

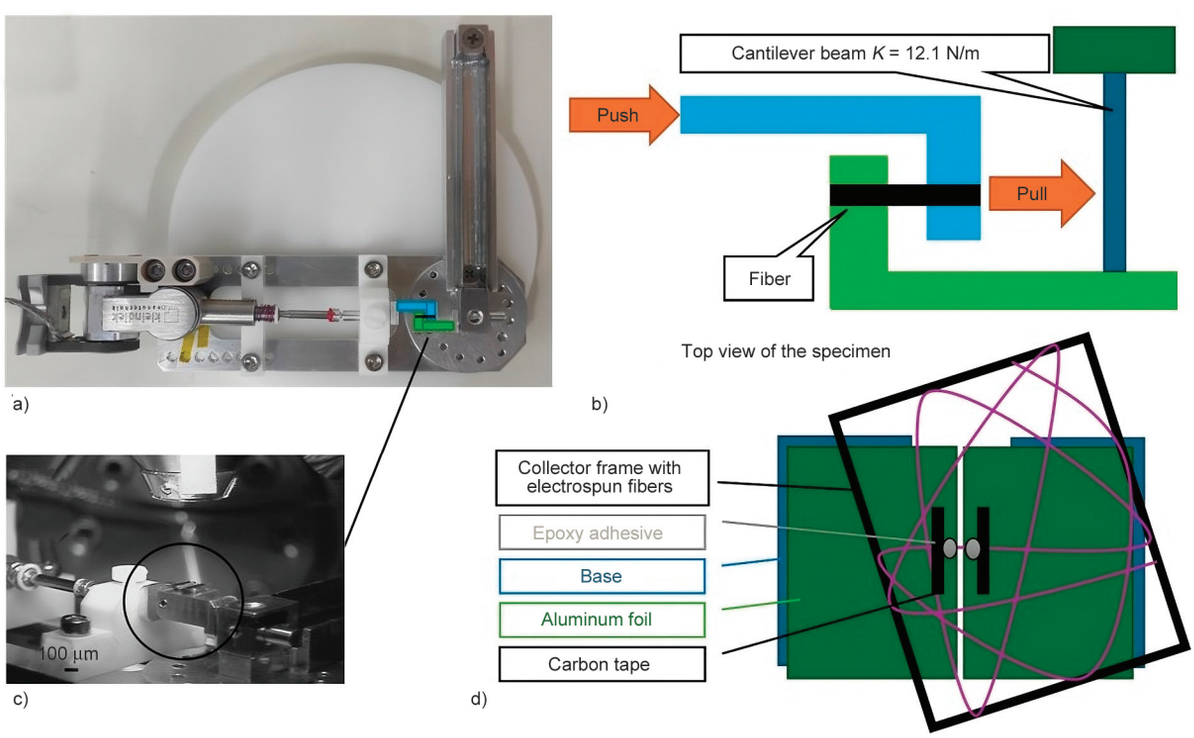

Figure 3. Homemade tensile testing device to measure sub-micron fibers; a) push-and-pull device, b) schematic structure of the device, c) the device fixed in the SEM chamber, d) specimen preparation and structure.

to the point of failure. ImageJ software was used to analyze the cantilever movement and the induced strain. As the displacement of the beam within the initial elastic range was too small to detect, Young's modulus could not be reliably estimated by this method. Therefore, we could not measure the modulus for sub-micron fibers.

2.4.3. Focused ion beam (FIB)

To measure the fracture toughness of epoxy fibers, a methodology was developed for inserting a well-defined notch in a thin fiber from which the crack should propagate spontaneously under tension, to obtain the critical force applied. For this purpose, we proposed to use a high-resolution field emission scanning electron microscope (FE-SEM) with the processing ability of a focused ion beam (FIB) to etch a particular notch shape within the fibers that will serve as an initiator for crack propagation. The FIB used here was Helios NanoLAB 600 (Thermo Fisher Scientific) equipped with AutoProbe™ 200 (OmniProbe).

A single fiber was placed on a silicon wafer, fixed at the edges with carbon tape, and then positioned in the FIB chamber. A location in the middle of the fiber was identified, and a condition as described in Table 1 was applied on a pattern of a linear line to create the notch. The notched fibers were then mounted on the push-to-pull device, and the same tensile procedure was conducted as described above.

3. Results

3.1. Molecular orientation

Polarized Raman analysis can detect molecular stress intensities in different directions of polarized light, providing insights into molecular morphology in two and three dimensions. Variations in intensities across different polarization modes indicate molecular orientation, particularly in the necking region along the fibers [19]. In this study, polarized micro-Raman analysis was conducted in two polarization modes: with the polarizer and analyzer both positioned either parallel (*ZZ*) or perpendicular (*XX*) to the longitudinal direction of the fiber surface (Figure 2a). This was performed on fibers with diameters of 2.0 and 5.5 μm to identify potential diameter size effects.

Table 1. Focused ion beam (FIB) conditions to etch a notch shape pattern within the fibers that will serve as an initiator for crack propagation.

Ion source	Gallium (Ga^+)
Acceleration voltage	30 kV
Extraction voltage	5.00 kV
Emission current	9.7 pA
Ion beam current	3.00 pA
Surface application	Si

Figure 4 presents the spectrum intensity of these fibers, using molded bulk epoxy as a reference. The bulk epoxy, representing an unstressed matrix, is expected to exhibit uniform stress intensities across different polarization modes. The bands related to the epoxy molecule backbone, which reflect molecular orientation, are primarily located between 1000 and 1700 cm^{-1} [19]. Key vibrations identified include the in-plane deformation and C–C stretching of the gem-dimethyl group of bisphenol A at 1184v, epoxide ring at 1255 cm^{-1}, aromatic ring stretching at 1610 cm^{-1}, aromatic C–H stretching and in-plane deformation at 1113 cm^{-1}, and C–H out-of-plane bending of the para-disubstituted phenyl group at 824 cm^{-1} [19]. Figure 4 demonstrates that both tested fibers exhibit higher intensity in the *ZZ* direction compared to the *XX* direction. Differences in stress intensities were quantified using the correlation (Equation (1)):

$$I = 1 - \frac{I_{xx}}{I_{yy}} \tag{1}$$

where I is the molecular orientation index, and I_{xx} and I_{zz} are the stress intensities in the lateral and longitudinal directions, respectively. High intensity indicates high molecular orientation in the analyzer direction, and vice versa. From Figure 4 we can see that the Intensity ratios are the same for most of the bonds, in this case we used the C–C stretching of gem-dimethyl group of bisphenol-A at 1184 cm^{-1} as a reference to quantify the intensities, as it is connected to the backbone's rigid molecular structure and should show consistency in direction during molecular orientation [22]. The 2.0 μm fiber exhibited a higher stress intensity ratio (I = 0.49) compared to the 5.5 μm fiber (I = 0.11), indicating greater molecular orientation in the thinner fiber. This observation highlights differences in molecular morphologies within the crosslinked matrix. Both fibers exhibited higher stress in the *ZZ* direction, which is the longitudinal direction (Figure 4). This likely results from the manufacturing process, where a viscous solution is drawn to form a fiber and held in place until solidification and full curing are achieved, inducing

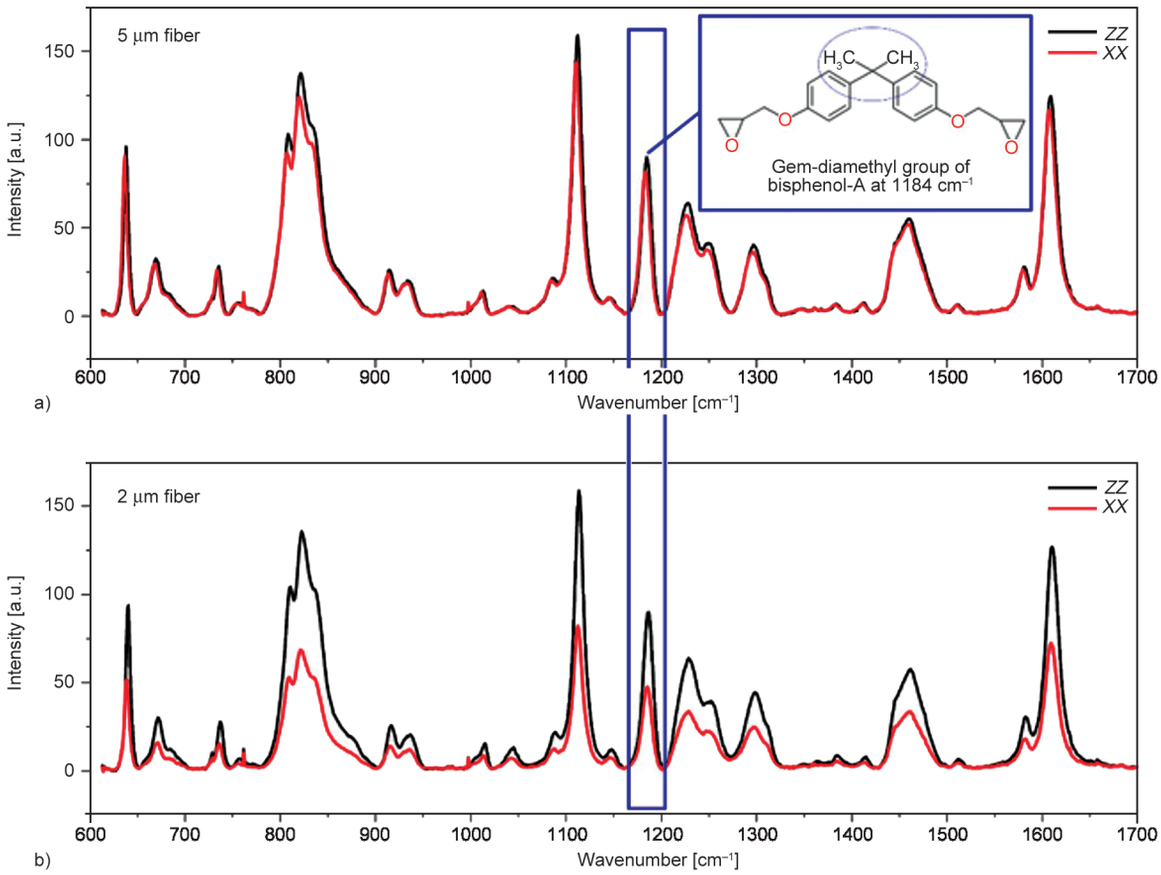

Figure 4. Polarized micro-Raman intensity analysis conducted over a wavelength range of 620–1700 cm^{-1} in both the lateral (*XX*) and longitudinal (*ZZ*) directions. The spectra represent the average results from 20 measured points taken along a 100 µm range in the longitudinal direction of the epoxy fiber. a) Fiber diameter of 5.5 µm and b) 2.0 µm.

molecular orientation along the drawing direction. These results suggest that molecular orientation exists in electrospun epoxy fibers and increases as the fibers become thinner, as seen in the 2.0 µm fiber compared to the thicker 5.5 µm fiber.

To further characterize the stress distribution along the fiber, Raman measurements were performed along a 100 µm long segment, allowing us to obtain the longitudinal orientation profile. Figures 5a and 5b show the differences in intensity along the fiber for the two polarizations and fiber thicknesses. The intensity along the fibers in the *ZZ* direction for both the 5.5 and 2.0 µm fibers is consistently higher than in the *XX* direction. The only observed deviation, in the 5.5 µm fiber, shows an overlap in intensities over a range of approximately 20 µm. It may point to areas that underwent relaxation, an effect that will be discussed later.

Figure 5c compares the stress intensity ratio, *I*, between the two tested fibers, providing insights into the orientation profile along the fiber. As previously mentioned, the 2.0 µm fiber exhibits higher orientation than the 5.5 µm fiber. Additionally, the intensity variations in the thinner fiber were significantly higher. In thinner fibers, the surface tension is more prominent due to the larger surface-to-volume ratio, making them more prone to diameter variations due to Plateau-Rayleigh instability, which may affect local molecular orientation along the fiber [23].

3.2. Mechanical properties

Stress-strain properties were measured by conducting tensile tests on three groups of epoxy fibers: (1) fibers mechanically drawn from a 30 wt% epoxy/MEK solution, with fiber diameters ranging from 7 to 80 µm, tested in previous research [18]; (2) fibers electrospun from a 30 wt% epoxy/MEK solution, yielding diameters ranging from 1.5 to 21 µm, also tested in previous research [18]; and (3) fibers electrospun from a 20 wt% epoxy/(DMF/THF) solution, which, due to its lower polymer concentration, produced much thinner fibers with diameters ranging from 150 nm to 5.5 µm. A previously tested group of molded epoxy bulk was used as a reference to

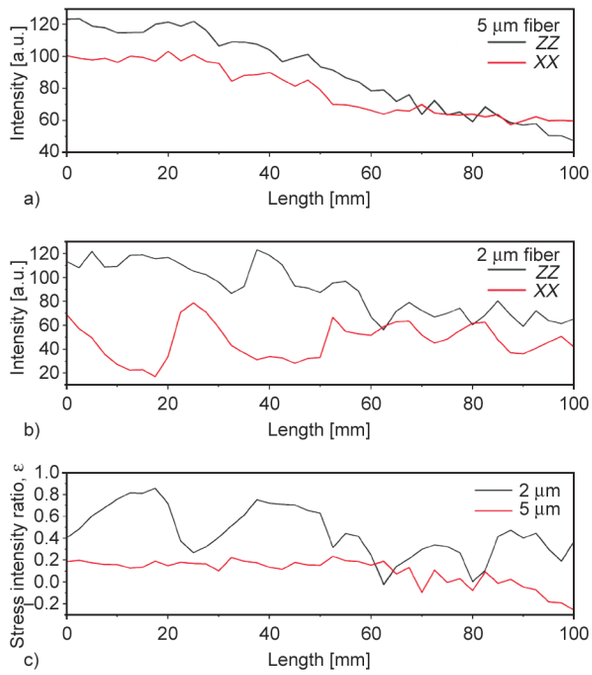

Figure 5. Polarized micro-Raman intensity analysis along fiber length of the 1184 cm^{-1} peak in epoxy fiber; *ZZ* and *XX* polarization of fibers in a) 5.5 µm and b) 2.0 µm diameter. c) Calculated stress intensity ratio, Equation (1). $I = 1 - I_{xx}/I_{zz}$, over a length of 100 µm along the fiber, as analyzed by Polarized micro-Raman. The readings were performed in 2.5 µm steps over a length of 100 µm along the sample.

represent an arbitrarily oriented molecular structure, demonstrating the mechanical properties of a matrix cured in a relaxed state [17].

The results for strength, strain at break, stiffness (Young's modulus), and effective toughness (the area under the stress-strain curve) of the different groups are presented and analyzed in Table 2. Tensile tests on the fibers revealed a trend of increasing strength as fiber diameter decreased (Figure 6a), with fibers demonstrating particularly high engineering strength, up to 978 MPa, and true strength of 1614 MPa for a fiber with a diameter of 411 nm, compared to 68 MPa for the molded bulk (Table 2). The scatter in the results is fairly wide, reflecting the large number of material and processing parameters intrinsic in this method; however, the trends of improvement in mechanical properties are evident. In general, the standard deviation increased as the fibers got thinner because of higher sensitivity to defects created during the process and handling. The strain versus fiber diameter correlation shows an average relative elongation range of 68–109%. This high elongation is uncharacteristic of epoxy, which is typically a brittle material with a maximum elongation of about 12%. Strain exhibited an interesting correlation with diameter; as shown in Figure 6b, it reached a maximum of 120% for fibers with diameters in the range of 2–12 µm but decreased as the fibers became either thicker or thinner. We assume that the necking propagation covers the fiber's full length because the strain range was, on average, double the length.

The elastic modulus of epoxy fibers with diameters ranging from 1.5 to 80 µm shows a clear diameter-dependent trend: as the fiber diameter decreased, the modulus increased (Figure 7). The thinnest group of fibers (20 wt% epoxy/THF/DMF solution) had an average elastic modulus of around 3.1 GPa, compared to just 1.1 GPa for bulk epoxy (Table 2). Differences in modulus for the same material can result from molecular orientation, as will be elaborated in the discussion.

To measure the fracture toughness of electrospun fibers, a notch was created by the FIB to initiate and monitor crack propagation. The results demonstrated that focused ion beam can etch effectively and produce a well-defined notch in the epoxy fiber (Figure 8). In tensile tests, notched epoxy fibers with a notch length comprising 20% of their total thickness exhibited plastic deformation before failure. Observations of fractured fibers revealed that

Table 2. Average engineering tensile properties of epoxy fibers using different processing techniques.

Processing technic	Solution	Diameter before tension [µm]	Diameter after tension [µm]	Yield strength [MPa]	Eng. strength [MPa]	True strength [MPa]	Strain at break [%]	Effective toughness [MPa]	Modulus [GPa]
Molding bulk [12]	Neat epoxy	–	–	–	68	–	12±2	5±1	1.13±0.65
Drawing [13]	Epoxy (30%)/MEK	28±18	–	48±16	61±21	–	68±28	29±19	2.37±0.65
Electrospinning [13]	Epoxy (30%)/MEK	7±3	–	55±20	121±64	–	109±13	63±35	2.07±0.57
Electrospinning	Epoxy (20%)/(DMF/THF)	1.77±0.91	1.03±0.39	71±49	201±189	399±385	74±30	–	3.15±0.96

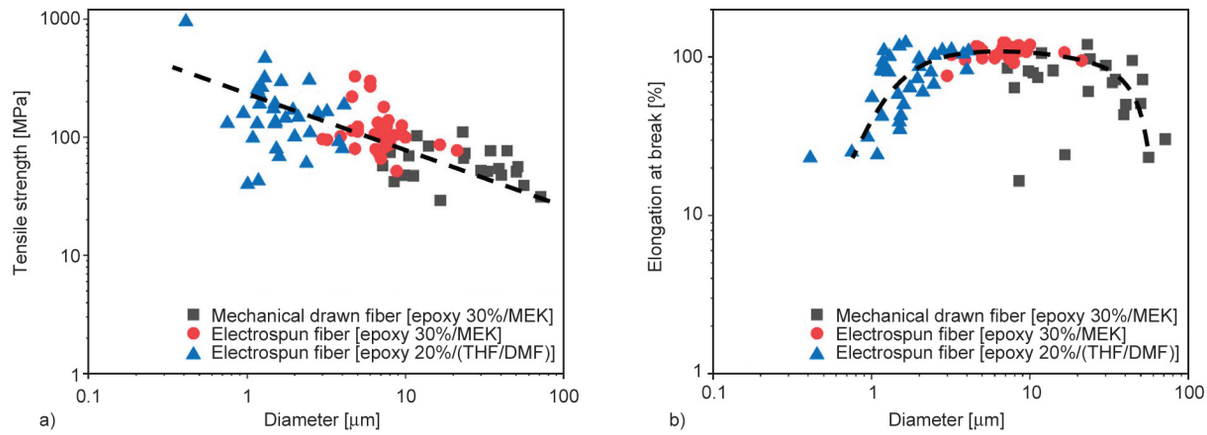

Figure 6. Engineering tensile properties of tensile strength (a) and elongation at break (b) at different epoxy fiber diameters. Three fiber groups were tested and presented: drawn fibers (black), electrospun fibers made from 30 wt% epoxy in the solution (red), and electrospun fibers made from 20 wt% epoxy in the solution (blue).

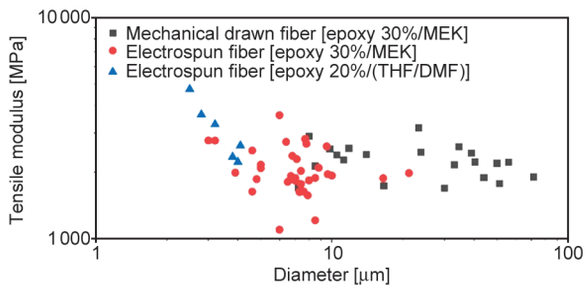

Figure 7. Tensile modulus at different fiber diameters. Three fiber groups were tested: drawn fibers made from 30 wt% epoxy in a solution (black), electrospun fibers made from 30 wt% epoxy in a solution (red), and electrospun fibers made from 20 wt% epoxy in a solution (blue).

fractures did not initiate at the notch but occurred at random locations along the fiber (Figure 8c). This phenomenon can be explained by the high energy dissipation capability of the fiber matrix due to its greatly increased plasticity, which practically makes the fiber crack insensitive.

4. Discussion

Tensile tests were conducted on electrospun epoxy fibers and compared with bulk epoxy specimens, resulting in the stress-strain curves shown in Figure 9. The tensile response of the fibers differs significantly from that of the bulk material. Bulk epoxy exhibits brittle characteristics with minimal plastic deformation, achieving an average failure strength of 68 MPa and a maximum strain of 12% [17]. By contrast, electrospun fibers demonstrate significant plastic deformation, maintaining a relatively constant strength before strain hardening occurs, leading to a much higher failure strain compared to the bulk.

Failure analysis using SEM of the electrospun epoxy fibers after tensile testing (Figure 10) reveals, in many fibers, the formation of separate long necking regions, indicating substantial plastic deformation, a behavior uncommon in epoxy, which typically shows only minimal, barely visible necking before failure. The appearance of separate necking regions along the fiber indicates multiple, process-induced weak points, each starting point for yield, which is the beginning of the molecular movement, and plastic deformation. The ductility of mechanically drawn micro epoxy fibers was described by Hobbiebrunken *et al.* [24], who also estimated the theoretical strength of about 265 MPa (10% of the modulus), which is close to our results, as shown in Table 2.

To explain the presence of plastic deformation in a naturally brittle material, it is crucial to consider the molecular morphology of the solution at three key stages: (1) just before fiber formation, (2) during electrospinning, as the solution transitions from liquid to solid, and (3) during the final relaxation and full curing stages.

Epoxy solution for electrospinning is in an early stage of crosslinking just prior to the gel point [21]. Molecular morphology is characterized by dissolved clusters of covalently crosslinked epoxy in a soluble state [20, 24]. Those clusters are large enough to interact with their neighbors, mainly via electrostatic chemical bonds, particularly hydrogen bonds, but not covalent bonds, and possibly marginal molecular overlaps that create local entanglements. The clusters get bigger as curing proceeds, increasing their interactions, thereby increasing the viscosity of the solution [20].

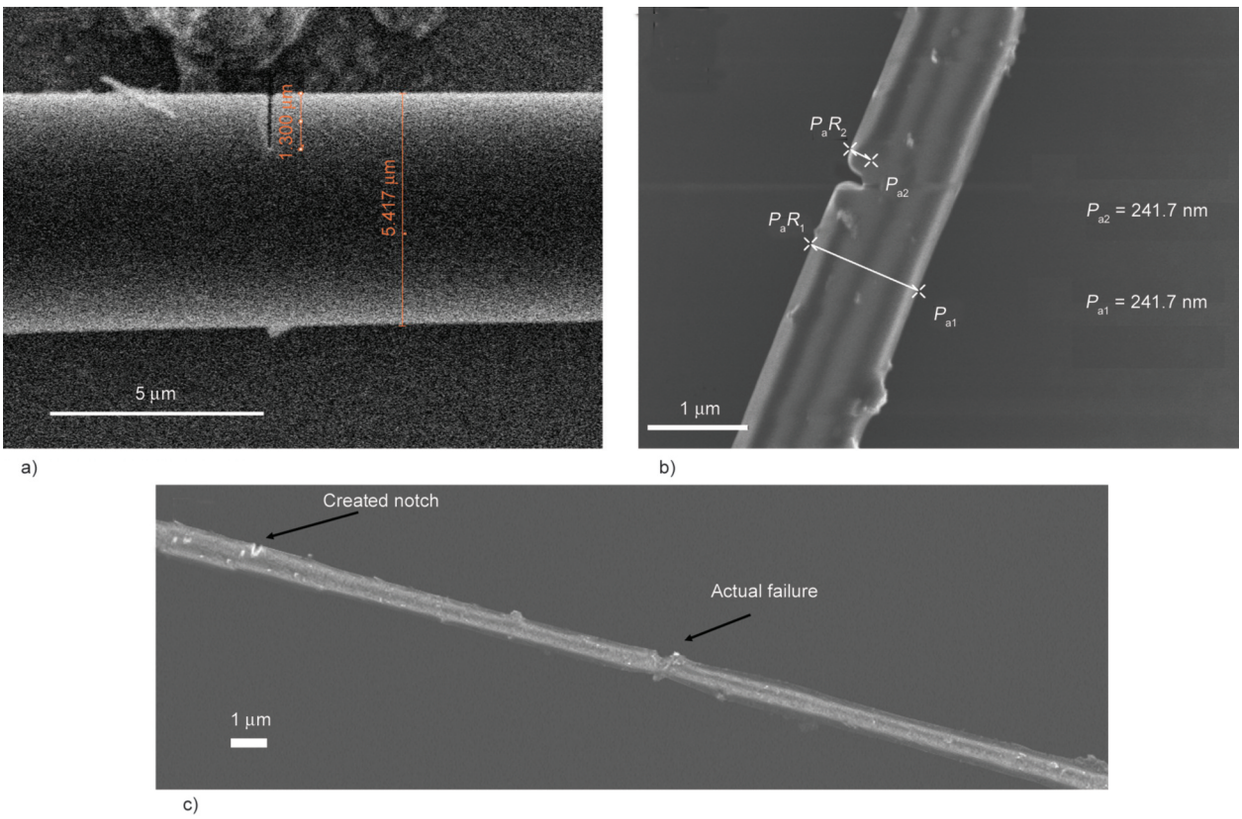

Figure 8. Fibers with a notch cut by focused Ion-beam (FIB) as seen in a high-resolution field emission scanning electron microscope (FE-SEM); Fibers with a diameter of a) 5.42 µm and b) 1.19 µm with well-defined notch shape and size. c) The fiber, as presented in Figure 8b, just before failure during the tensile test in the SEM chamber.

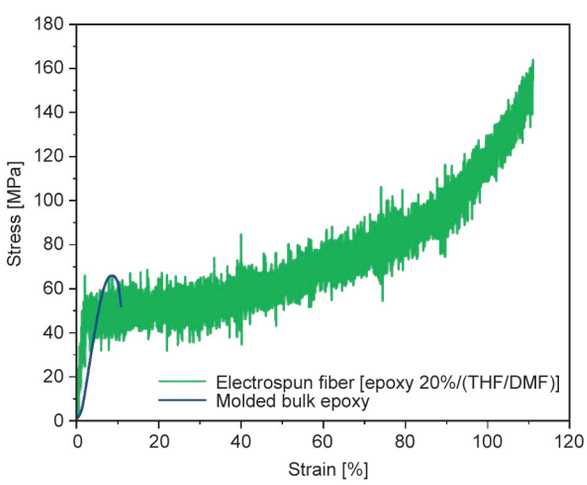

Figure 9. Engineering stress-strain curves of a representative molded epoxy bulk and electrospun fiber with a diameter of 3.2 µm. The force readings for the fiber exhibited high instability, particularly at low force values. This is likely due to the instrument operating near its tolerance limit.

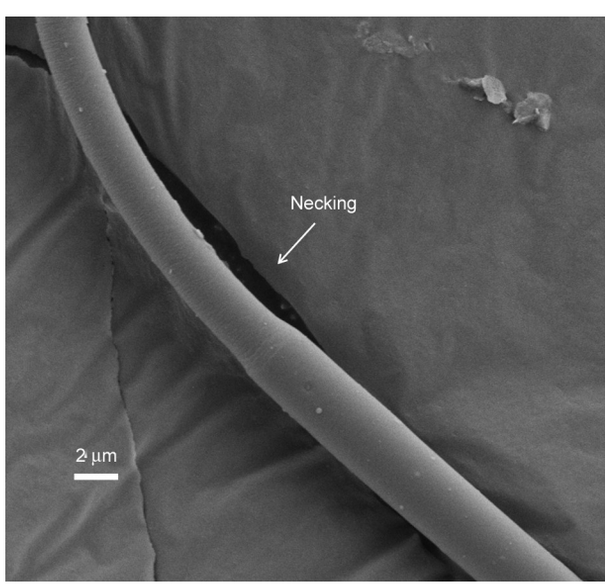

Figure 10. SEM micrograph of an electrospun epoxy fiber after tensile test.

During electrospinning, the viscous solution is injected into a high electric field, where it is rapidly stretched by electrostatic forces driven by the dielectric solvent, initiating fiber formation [20]. As shown schematically in Figure 11a, the solution's molecular morphology aligns with the drawing direction due to the generation of strong shearing forces [25]. Simultaneously, rapid solvent evaporation from the stretched fiber reduces free volume and accelerates the curing process while the fiber remains under tension [25]. This continuous stretching, coupled with

fast chemical crosslinking, locks the molecular structure into an oriented configuration, resulting in a unique molecular morphology.

Upon reaching the collector, the fiber is typically in a gel state or even vitrified; otherwise, it would revert to a viscous droplet. The crosslinking reaction slows down significantly at this stage due to the reduced molecular diffusion rate, thereby preserving the cluster-oriented morphology [20]. As the fiber partially relaxes on the collector, crosslinking continues at a slower pace, converting the clusters into nodules—a solid-state form of the cluster morphology [26–28]. This significant relaxation process is depicted in Figure 11a.

Previous research has shown that only a third of the total crosslinking reaction occurs by the time the gel point is reached [21], meaning that the fiber matrix has a low crosslinking ratio at this stage, with residual solvent, free epoxy monomers, and polymerized epoxy fragments facilitating rapid and extensive relaxation. Once the electrospun epoxy fiber is created and reaches the collector, the stretching forces cease, allowing it to relax at the early matrix gel point as it keeps slowly crosslinking. At this point, the clusters convert to nodules, a solid state of the cluster morphology.

After full curing in an oven, the molecular orientation of the fibers was assessed using polarized micro-Raman spectroscopy. The results showed higher intensities along the fiber's longitudinal direction, with ratios of $I_{5.5\ \mu m} = 0.11$ and $I_{2.0\ \mu m} = 0.49$, as described in the experimental section, indicating longitudinal orientation. The thinner fibers exhibited a higher degree of orientation, likely due to faster solvent evaporation, a phenomenon associated with high surface energy, which is more pronounced in thinner fibers [29]. Furthermore, the thinner fibers underwent stronger stretching during the electrospinning, and therefore their molecular conformation was more elongated and oriented, and consequently, subsequent relaxation was restrained.

The unique molecular morphology created during epoxy electrospinning facilitates significant plastic deformation, characterized by the necking effect (Figure 10), which is common in thermoplastic polymers but unusual in thermosets such as epoxy. As discussed, this effect results from the specific processing conditions during electrospinning, where

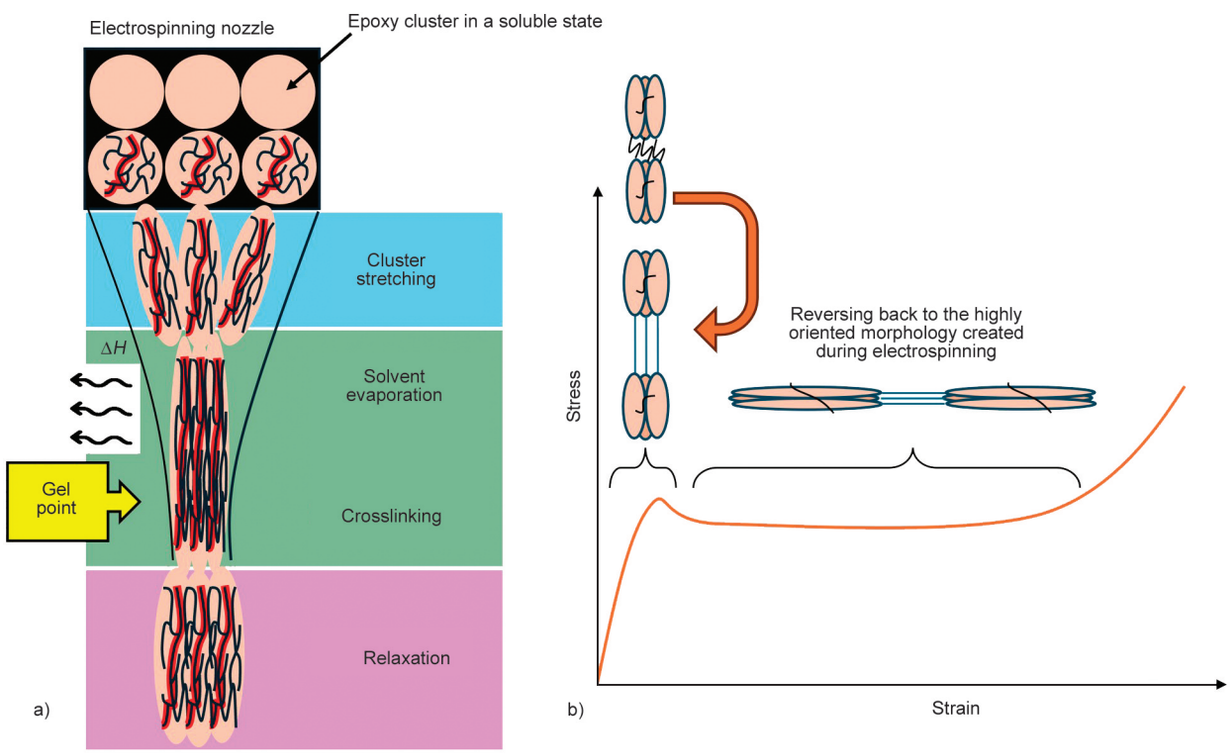

Figure 11. a) Schematic illustration of the molecular epoxy matrix morphology during the electrospinning process. b) Tensile test effect on the nodular structure of electrospun fully cured epoxy fibers. (i) The cluster in soft matter converts to a nodule in the solid state, a nodular structure with slight orientation, which is preserved after processing and relaxation. (ii) The cross-linked nodular structure reverts to the post-gel molecular morphology, which is characterized by high cluster stretching with minimal stretch on the external crosslinking.

molecular fixation occurs through crosslinking until the gel point. It is important to note that the final molecular morphology of the matrix is established at the gel point (Figure 11a). After the fiber is formed, it undergoes relaxation while resting on the collector, yet the morphology remains as it was at the gel point. When tensile force is applied on the fiber, elastic deformation occurs, stretching and orienting the clusters and the surrounding regions with lower crosslink density, as illustrated in Figure 11b. As the force increases, the fibers plastically deform. This plastic deformation coincides with the reversion of the molecular morphology to its pre-relaxation structure, allowing substantial plastic deformation (Figure 11b) up to the limit of extensibility, where clusters and crosslinked regions are fully stretched [30].

Beyond this point, continued application of force induces strain hardening in the matrix. This stage is characterized by a significant increase in strength, driven by high molecular orientation [31].

The average modulus of the fibers was found to be up to 3 GPa, compared to 1.1 GPa for the molded bulk material, as shown in Table 2. Notably, the modulus increased as the fiber thickness decreased. This increase in modulus is likely due to the alignment of molecular chains, which creates order in a specific direction, reduces free space between molecules, and constrains their mobility, leading to lower plasticity and higher modulus, as supported by polarized Raman analysis [19].

Strain-to-failure analysis of the electrospun fibers, as presented in Figure 6b, revealed interesting results. The fibers achieved a strain of 120% within a diameter range of 2–7 μm; therefore, we can assume that all the fiber was plastically deformed, but as the fiber diameter decreased further, the strain to failure also decreased. Consequently, the fibers show lower strain at break as they get thinner, because most of the strain is already integrated within the crosslinked matrix, as demonstrated in the Raman analysis for different diameters of fibers and described in Figure 11 [19].

Comparing the tensile properties of electrospun fibers and molded bulk epoxy clearly indicates that the processing conditions during the epoxy crosslinking reaction – whether through electrospinning or molding – critically affect the modulus, strain, and strength of the final product. This is due to the formation of a distinct molecular morphology created during the crosslinking reaction, which takes place parallel to stress application.

We conducted fracture toughness tests to examine fracture propagation characteristics. The results showed that despite the presence of an initial notch of up to 20% of the total fiber diameter, all tested fibers failed at locations other than the notched area, without initiating a brittle fracture.

In bulk brittle epoxy with a notch, failure typically occurs at the notch tip, where fracture propagation begins due to the matrix's low energy dissipation capacity [32, 33]. In brittle epoxy, elastic energy released due to crack extension may exceed the material fracture energy and cause crack propagation until fracture [34].

In contrast, the fibers tested in this study exhibited ductility, allowing the matrix to undergo plastic deformation, which relaxes stresses at the crack tip. To account for this ductility, we applied Irwin's models to introduce a singularity-dominated zone, estimate its size, and evaluate the elastic-plastic boundary. According to Irwin, the normal stress (σ) at the crack tip in a linear elastic material is given by Equation (2), [34]:

$$\sigma_Y = \frac{K_{IC}}{F\sqrt{2\pi r_p}} \tag{2}$$

where K_{IC} is the critical stress intensity factor for opening mode, F is a dimensionless constant that depends on specimen geometry, and r_p is the size of the singularity-dominated zone in which yielding of ductile materials occurs when σ_Y is exceeded. A long, thin fiber can be viewed approximately as being in a plane stress condition.

To adapt this model for the cylindrical fiber geometry, we used the geometrical parameter F for a surface crack in a solid cylinder, developed by Foemen and Shivakumar [35] and described by the following correlation, Equation (3):

$$F = G\left[0.752 + 1.286\beta + 0.37Y^3\right] \tag{3}$$

where the parameters of $\beta = \frac{\pi}{2}\frac{a}{D}$, $Y = 1 - \sin\beta$, and $G = 0.92\left(\frac{2}{\pi}\right)^2 \sec\beta\left(\frac{\tan\beta}{\beta}\right)^{-\frac{1}{2}}$.

In these equations, a is the crack size and D is the fiber diameter. This geometrical factor provides a reasonable approximation, although it may not fully match our case. In our experiment, the crack created by FIB is a straight line, differing from the curved

crack used in the cylindrical case (Figure 12 inset). Therefore, the calculation of F provides a good approximation, but not exact. Solving Equation (2) for r_p and substituting the geometrical parameter F in Equation (3) yields an estimation of the elastic zone size around the crack tip for the fiber Equation (4):

$$r_p = \frac{1}{2\pi}\left[\frac{K_{IC}}{\sigma_Y G\left(0.752 + 1.286\beta + 0.37Y^3\right)}\right]^2 \quad (4)$$

This model allows us to estimate the size of the plastic zone under critical stress intensity conditions necessary for fracture propagation in the fiber. To calculate the plastic zone size (r_p) of the epoxy fiber matrix under these critical conditions, we used a K_{IC} value of 1.33 MPa·$\sqrt{m}$ from previous research on molded epoxy as a reference [36]. The actual K_{IC} values for the fiber should be different because they depend on many parameters that were not checked in this case, such as modulus and epoxy crosslinking density [32]. For example, for a fiber diameter of D = 1.19 µm, with an FIB-cut fracture length of a = 214 nm, and a yield stress of σ_Y = 71 MPa (Table 2), the calculated singularity-dominated zone is r_p = 93 µm (Figure 12). This result suggests that the plastic zone is much larger than the diameter of the fiber. Consequently, when tensile forces are applied to a fiber thinner than 93 µm, the stress at the crack tip disperses throughout the entire fiber diameter, making the stress distribution uniform along the fiber, equal to the yield stress. Once yielding spreads along the fiber, failure can occur in regions where the local strain exceeds the ultimate strain, most likely at weak points such as narrower diameter, local porosity, or local distortions.

5. Conclusions

The present study demonstrates that electrospinning is a promising technique for producing epoxy fibers at the nanometric scale with superior mechanical properties. The mechanical testing of these electrospun epoxy fibers revealed ductile behavior, contrasting with the brittle nature of molded bulk epoxy. Notably, the tensile tests indicated a significant increase in both strength and modulus as the fiber diameter decreased.

This change in mechanical properties is attributed to the distinct molecular morphology formed during electrospinning, compared to that in molded bulk epoxy. Unlike the molded bulk, where the solution remains at rest, electrospinning involves stretching at a high strain rate and rapid crosslinking. These processes fix the molecular structure into a nodular-oriented configuration. As the solution reaches the gel point during electrospinning, this quick transition to a solid state preserves the stretched molecular

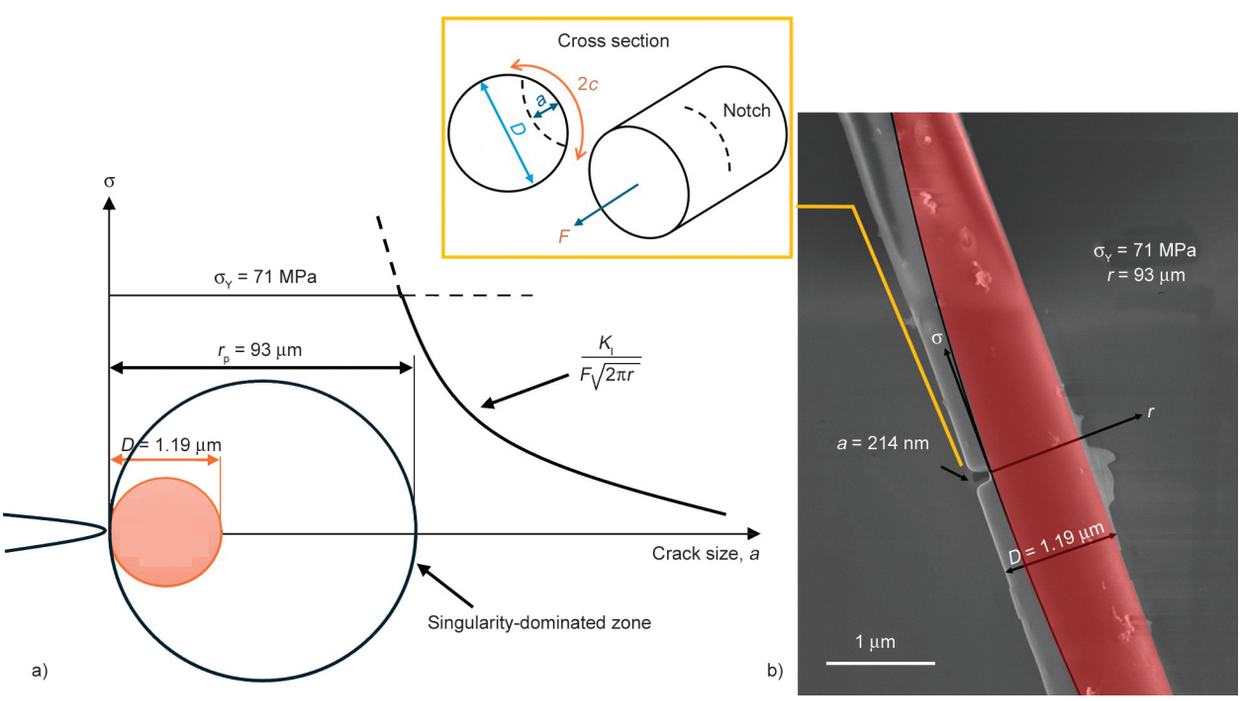

Figure 12. a) Distribution of the stress at the crack tip normal to the crack plane, and b) representative of epoxy electrospun fiber with a notch made by focused ion beam microscopy, the covered area in red describes the plastic zone area of size 93 µm for a notch to diameter ratio of 18%.

morphology, as supported by polarized micro-Raman orientation analysis.

Furthermore, the fibers experience significant relaxation, which acts as a plastic deformation region. Upon the application of tensile force, the molecular structure reverts to its pre-relaxation, stretched state, enabling further plastic deformation. This unique molecular morphology, resulting from the specific processing conditions of electrospinning, imparts ductile properties to the epoxy matrix.

Acknowledgements

This research was supported in part by the Israel Science Foundation (grant #2439/19), and by the generosity of the Harold Perlman family. The authors would like to thank the Moskowitz Center for Nano and Bio-Imaging funding for supporting the in-situ mechanical testing device under the SEM.

References

[1] Jian S., Zhu J., Jiang S., Chen S., Fang H., Song Y., Duan G., Zhang Y., Hou H.: Nanofibers with diameter below one nanometer from electrospinning. RSC Advances, **8**, 4794–4802 (2018). https://doi.org/10.1039/C7RA13444D

[2] Ji D., Lin Y., Guo X., Ramasubramanian B., Wang R., Radacsi N., Jose R., Qin X., Ramakrishna S.: Electrospinning of nanofibres. Nature Reviews Methods Primers, **4**, 1 (2024). https://doi.org/10.1038/s43586-023-00278-z

[3] Ding J., Li T., Wang X., Li M., Li T., Zhang Z.: Preparation of functionalized ethylene–vinyl-alcohol nanofibrous membrane filter for rapid and cyclic removing of organic dye from aqueous solution. Polymers, **16**, 2328 (2024). https://doi.org/10.3390/polym16162328

[4] Liu H., Zhu Y., Zhang C., Zhou Y., Yu D-G.: Electrospun nanofiber as building blocks for high-performance air filter: A review. Nano Today, **55**, 102161 (2024). https://doi.org/10.1016/j.nantod.2024.102161

[5] Rocco K. A., Maxfield M. W., Best C. A., Dean E. W., Breuer C. K.: *In vivo* applications of electrospun tissue-engineered vascular grafts: A review. Tissue Engineering Part B: Reviews, **20**, 628–640 (2014). https://doi.org/10.1089/ten.TEB.2014.0123

[6] Zhang X., Wang Y., Gao Z., Mao X., Cheng J., Huang L., Tang J.: Advances in wound dressing based on electrospinning nanofibers. Journal of Applied Polymer Science, **141**, e54746 (2024). https://doi.org/10.1002/app.54746

[7] Xia Q., Wang C., Yang B., Li M., Han W., Chen H.: Study on the melt electrospinning method with internal electrode and fiber refinement. Fibers and Polymers, **26**, 1519–1528 (2025). https://doi.org/10.1007/s12221-025-00897-1

[8] Dai S., Liang H., Zhu M., Zhang Y.: Electrospun silk for biomedical applications. Med-X, **2**, 22 (2024). https://doi.org/10.1007/s44258-024-00038-y

[9] Rostami M., Beheshtizadeh N., Ranjbar F. E., Najafi N., Ahmadi A., Ahmadi P., Rostamabadi H., Pazhouhnia Z., Assadpour E., Mirzanajafi-Zanjani M., Kisomi M. F., Kharazmi M. S., Jafari S. M.: Recent advances in electrospun protein fibers/nanofibers for the food and biomedical applications. Advances in Colloid and Interface Science, **311**, 102827 (2023). https://doi.org/10.1016/j.cis.2022.102827

[10] Ura D. P., Stachewicz U.: Direct electrospinning of short polymer fibers: Factors affecting size and quality. Composites Part A: Applied Science and Manufacturing, **181**, 108138 (2024). https://doi.org/10.1016/j.compositesa.2024.108138

[11] Enns J. B., Gillham J. K.: Time–temperature–transformation (TTT) cure diagram: Modeling the cure behavior of thermosets. Journal of Applied Polymer Science, **28**, 2567–2591 (1983). https://doi.org/10.1002/app.1983.070280810

[12] Rubinstein M., Colby R. H.: Polymer physics. Oxford University Press, Oxford (2003).

[13] Flory P. J.: Molecular size distribution in three dimensional polymers. I. Gelation. Journal of the American Chemical Society, **63**, 3083–3090 (1941). https://doi.org/10.1021/ja01856a061

[14] Fekiač J. J., Krbata M., Kohutiar M., Janík R., Kakošová L., Breznická A., Eckert M., Mikuš P.: Comprehensive review: Optimization of epoxy composites, mechanical properties, & technological trends. Polymers, **17**, 271 (2025). https://doi.org/10.3390/polym17030271

[15] Aziz T., Haq F., Farid A., Cheng L., Chuah L. F., Bokhari A., Mubashir M., Tang D. Y. Y., Show P. L.: The epoxy resin system: Function and role of curing agents. Carbon Letters, **34**, 477–494 (2024). https://doi.org/10.1007/s42823-023-00547-7

[16] Ou B., Wang Y., Lu Y.: A review on fundamentals and strategy of epoxy-resin-based anticorrosive coating materials. Polymer-Plastics Technology and Materials, **60**, 601–625 (2021). https://doi.org/10.1080/25740881.2020.1819317

[17] Sui X., Tiwari M., Greenfeld I., Khalfin R. L., Meeuw H., Fiedler B., Wagner H. D.: Extreme scale-dependent tensile properties of epoxy fibers. Express Polymer Letters, **13**, 993–1003 (2019). https://doi.org/10.3144/expresspolymlett.2019.86

[18] Shneider M., Sui X. M., Greenfeld I., Wagner H. D.: Electrospinning of epoxy fibers. Polymer, **235**, 124307 (2021).
https://doi.org/10.1016/j.polymer.2021.124307

[19] Sui X., Pinkas I., Wagner H. D.: A polarized micro-Raman study of necked epoxy fibers. Polymer, **230**, 124034 (2021).
https://doi.org/10.1016/j.polymer.2021.124034

[20] Greenfeld I., Shneider M., Kaestner A., Wagner H. D.: Stiffness modeling of thermoset polymer fibers. Journal of Polymer Science, **62**, 1533–1543 (2024).
https://doi.org/10.1002/pol.20240082

[21] Shneider M., Zattelman R., Kaestner A., Greenfeld I., Wagner H. D.: Electrospinning of epoxy fibers: Effect of curing conditions on solution rheological behavior. Journal of Applied Polymer Science, **140**, e54437 (2023).
https://doi.org/10.1002/app.54437

[22] Talele T. T.: Natural-products-inspired use of the gem-dimethyl group in medicinal chemistry. Journal of Medicinal Chemistry, **61**, 2166–2210 (2017).
https://doi.org/10.1021/acs.jmedchem.7b00315

[23] Tanaka M., Young R. J.: Review polarised Raman spectroscopy for the study of molecular orientation distributions in polymers. Journal of Materials Science, **41**, 963–991 (2006).
https://doi.org/10.1007/s10853-006-6595-7

[24] Hobbiebrunken T., Fiedler B., Hojo M., Tanaka M.: Experimental determination of the true epoxy resin strength using micro-scaled specimens. Composites Part A: Applied Science and Manufacturing, **38**, 814–818 (2007).
https://doi.org/10.1016/j.compositesa.2006.08.006

[25] Greenfeld I., Fezzaa K., Rafailovich M. H., Zussman E.: Fast X-ray phase-contrast imaging of electrospinning polymer jets: Measurements of radius, velocity, and concentration. Macromolecules, **45**, 3616–3626 (2012).
https://doi.org/10.1021/ma300237j

[26] Kreibich U. T., Schmid R.: Inhomogeneities in epoxy resin networks. Journal of Polymer Science: Polymer Symposia, **53**, 177–185 (1975).
https://doi.org/10.1002/polc.5070530122,

[27] Dušek K., Pleštil J., Lednický F., Luňák S.: Are cured epoxy resins inhomogeneous? Polymer, **19**, 393–397 (1978).
https://doi.org/10.1016/0032-3861(78)90243-4

[28] Sahagun C. M., Morgan S. E.: Thermal control of nanostructure and molecular network development in epoxy-amine thermosets. ACS Applied Materials and Interfaces, **4**, 564–572 (2012).
https://doi.org/10.1021/am201515y

[29] Asha A. B., Narain R.: Nanomaterials properties. in 'Polymer science and nanotechnology' (ed.: Narain R.) Springer, Cham, 343–359 (2020).
https://doi.org/10.1016/B978-0-12-816806-6.00015-7

[30] Ward I. M., Sweeney J.: Mechanical properties of solid polymers. Wiley, Chichester (2012).

[31] Robertson R. E.: Theory for the plasticity of glassy polymers. The Journal of Chemical Physics, **44**, 3950–3956 (1966).
https://doi.org/10.1063/1.1726558

[32] Levita G., de Petris S., Marchetti A., Lazzeri A.: Crosslink density and fracture toughness of epoxy resins. Journal of Materials Science, **26**, 2348–2352 (1991).
https://doi.org/10.1007/BF01130180

[33] Goldberg O., Greenfeld I., Wagner H. D.: Efficient toughening of short-fiber composites using weak magnetic fields. Materials, **13**, 2415 (2020).
https://doi.org/10.3390/ma13102415

[34] Anderson T. L.: Fracture mechanics: Fundamentals and applications. CRC Press, Boca Raton (2005).

[35] Forman R. G., Shivakumar V.: Growth behavior of surface cracks in the circumferential plane of solid and hollow cylinders. in 'Fracture mechanics: Seventeenth volume' (eds.: Underwood J. H., Chait R., Smith C. W., Wilhem D. P., Andrews W. R., Newman J. C.) ASTM International, West Conshohocken, 1–18 (1986).
https://doi.org/10.1520/STP17388S

[36] Lachman N., Wagner H. D.: Correlation between interfacial molecular structure and mechanics in CNT/epoxy nano-composites. Composites Part A: Applied Science and Manufacturing, **41**, 1093–1098 (2010).
https://doi.org/10.1016/j.compositesa.2009.08.023